Dispersion and Nonlinear Phase-Shift Compensation in High-Peak-Power Short-Pulse Fiber Laser Sources Using Photonic-Crystal Fibers

E. E. Serebryannikov[a], A. M. Zheltikov[a],*, K.-H. Liao[b], A. Galvanauskas[b], and A. Baltuška[c]

[a] Physics Department, International Laser Center, Moscow State University, Moscow, 119992 Russia
[b] Center for Ultrafast Optical Science, University of Michigan, Ann Arbor, MI 48109-2122, USA
[c] Institute of Photonics, Vienna University of Technology, Gusshausstrasse 27/387, Vienna, 1040 Austria
*e-mail: zheltikov@phys.msu.ru
Received February 25, 2008

Abstract—Photonic-crystal fibers (PCFs) with a specifically designed dispersion profile and nonlinearity are shown to enable an accurate broadband compensation of the stretcher–compressor dispersion in fiber laser sources of high-peak-power ultrashort light pulses. We demonstrate that the nonlinear phase shift in such systems can partially compensate for the fourth-order dispersion, allowing the stretcher–compression group delay to be compensated up to the fourth-order dispersion terms by using a sequence of only two fibers—a standard optical fiber and a PCF.

1. INTRODUCTION

Photonic-crystal fibers (PCFs) [1–4] offer an unprecedented control over waveguide dispersion. The PCF design allows the wavelength of zero group-velocity dispersion (GVD) to be tuned within a broad spectral range [5], making it possible to directly couple a Ti:sapphire laser output into solitons in the fiber [6] and providing phase matching for a broad class of parametric four-wave mixing processes [7]. Combined with a high optical nonlinearity, provided by PCFs with very small cores and high core-cladding index steps [1, 8], the unique dispersion flexibility of the PCFs enables a radical enhancement of the nonlinear-optical transformation for laser fields with broadly varying parameters from the countinuous-wave radiation [9] to few-cycle laser pulses [10]. PCF-based supercontinuum radiation sources [11, 12] and frequency converters [7] are widely employed in optical metrology [13–16], show a tremendous potential for improving the performance of optical coherence tomographs [17], as well as nonlinear spectrographs [18, 19] and microscopes [20–22] based on coherent anti-Stokes Raman scattering (CARS). Such fiber components serve as an ultrafast flash in time-resolved spectroscopy [23] and expand the applicability range of femtosecond laser sources to photochemistry and photobiology [8]. In advanced laser sources of few-cycle light pulses, PCFs are widely employed nowadays to control the carrier–envelope phase (CEP) of few-cycle field waveforms [13, 24], enabling the generation of isolated attosecond pulses [25], leading to the development of new methods of spectroscopy with attosecond time resolution [26], and facilitating the creation of extreme-intensity laser systems [27] and frequency comb synthesizers for high-precision measurements [28].

In laser technologies, the tailored dispersion of PCFs helps to balance the group delay inside fiber oscillators [29–34], as well as to amplify [35], spectrally broaden [36], and compress [36, 37] high-peak-power laser output. An all-fiber chirped-pulse amplification system based on compression in an air-guiding photonic band-gap fiber has been demonstrated by Limpert et al. [37]. As shown by de Matos et al. [38], hollow-core PCFs allow the creation of all-fiber pulse compressors for high-peak-power pulses within a broad range of wavelengths.

Photonic-crystal fibers also contributed to the power scaling using fiber lasers. Since the precision of the tailoring PCF waveguide parameters during fiber fabrication exceeds that of conventional index-guiding fibers, a very large core single-mode PCF supporting a single mode (with $V < \pi$) can be fabricated [37]. Such PCFs complement the existing fiber laser technologies [38, 39]. Large mode-area PCF components [40, 41] have been shown to allow the creation of high-power fiber lasers [42, 43], the amplification of a short-pulse fiber laser output [35], the compression of submegawatt, subpicosecond laser pulses [36], and the efficient supercontinuum generation for high-energy nanosecond [44] and femtosecond [45] laser pulses.

The accurate design of a PCF dispersion profile for the precise dispersion compensation through fiber structure engineering is key to optimizing the performance of fiber laser sources of ultrashort light pulses. Here, we show that, for a broad class of fiber laser oscillator–amplifier systems involving pulse stretching,

chirped-pulse amplification, and pulse compression, the nonlinear phase shift can partially compensate for the fourth-order dispersion. We also propose a conveniently formalized algorithm for the design of the PCF dispersion in fiber laser systems allowing the dispersion of a stretcher–compressor system to be compensated to the fourth order by using a sequence of only two fibers—a standard passive fiber and a PCF with a carefully designed dispersion profile. We present examples of the pulse evolution in such stretcher–compressor systems demonstrating the performance of optimized PCF-based stretchers in fiber oscillator–amplifier sources of ultrashort high-peak-power light pulses.

2. DESIGN RULE FOR A COMPOSITE FIBER PULSE STRETCHER

We consider a generic fiber laser system consisting of a fiber oscillator, stretcher, amplifier, and a compressor. The group delay introduced by the compressor $G_c(\omega)$ is represented as a Taylor series about the central frequency ω_0:

$$G_c(\omega) = \frac{\partial \varphi_c(\omega)}{\partial \omega} \approx \theta_1 + \theta_2(\omega - \omega_0)$$
$$+ \frac{\theta_3}{2}(\omega - \omega_0)^2 + \frac{\theta_4}{6}(\omega - \omega_0)^3 + \dots, \quad (1)$$

where φ_c is the phase shift introduced by the compressor and $\theta_k = (\partial^k \varphi_c / \partial \omega^k)|_{\omega_0}$.

The stretcher should then be designed in such a way so as to precompensate for group delay (1) within the required range of frequencies ω. Mathematically, this condition implies that the group delay introduced by the stretcher $G_s(\omega)$ should reproduce the frequency profile of $-G_c(\omega)$ with minimum deviations within the considered frequency interval.

A stretcher that consists of a sequence of M fibers supporting guided modes with propagation constants $\beta^{(m)}$, $m = 1, 2, \dots, M$, gives rise to the group delay

$$G_s(\omega) = \sum_{m=1}^{M} G_m(\omega) l_m, \quad (2)$$

where $G_m(\omega)$ is the group delay introduced by the mth fiber and l_m is the length of the mth fiber.

The expansion of $G_m(\omega)$ as a Taylor series about ω_0 yields

$$G_m(\omega) \approx \left[\frac{1}{u_m} + \beta_{2m}(\omega - \omega_0) + \frac{\beta_{3m}}{2}(\omega - \omega_0)^2 \right.$$
$$\left. + \frac{\beta_{4m}}{6}(\omega - \omega_0)^3 + \dots \right] l_m, \quad (3)$$

where $u_m = (\partial \beta^{(m)} / \partial \omega)_{\omega_0}^{-1}$ is the group velocity at the central frequency ω_0 and $\beta_{km} = (\partial^k \beta^{(m)} / \partial \omega^k)_{\omega_0}$.

It can be seen from Eqs. (1)–(3) that, to compensate for the stretcher–compressor dispersion up to the qth-order terms in the absence of nonlinear phase shifts, the stretcher should be designed in such a way so as to meet the following set of $q - 1$ linear equations:

$$\sum_{m=1}^{M} \beta_{pm} l_m^{(1)} = -\theta_p, \quad (4)$$

where $p = 2, 3, \dots, q$. Equation (4) constitutes the first step in our iterative procedure, indicated by subscript (1). At this step, we consider a purely linear regime of pulse stretching. Nonlinear phase shifts will be included through the next iterations of our procedure.

With $M = q - 1$, the number of unknowns in set (4) is equal to the number of equations. In this case, set (4) can be easily resolved with respect to the lengths of fibers $l_m^{(1)}$ in the stretcher unless the determinant of the $M \times M$ matrix $\hat{\beta}_{pm}$ is zero. The solution is given by

$$l_i^{(1)} = \frac{\Gamma_i^{(1)}}{\Gamma}, \quad (5)$$

where

$$\Gamma = \det(\beta_{pm}) \neq 0 \quad (6)$$

is the determinant of the $\hat{\beta}_{pm}$ matrix and

$$\Gamma_i^{(1)} = \begin{vmatrix} \beta_{21} & \dots & \beta_{2i-1} & -\theta_2 & \beta_{2i+1} & \dots & \beta_{2M} \\ \beta_{31} & \dots & \beta_{3i-1} & -\theta_3 & \beta_{3i+1} & \dots & \beta_{3M} \\ \dots & \dots & \dots & \dots & \dots & \dots & \dots \\ \beta_{q1} & \dots & \beta_{qi-1} & -\theta_q & \beta_{qi+1} & \dots & \beta_{qM} \end{vmatrix} \quad (7)$$

is the determinant of the matrix obtained from $\hat{\beta}_{pm}$ by replacing the ith column by the column composed of the free terms $-\theta_p$ in set of Eqs. (4).

Although, formally, Eqs. (4) can be resolved with respect to $l_m^{(1)}$ whenever $M = q - 1$ and $\Gamma \neq 0$, the solution of Eqs. (4) corresponds to the fiber lengths in a stretcher only when $l_m^{(1)} \geq 0$ for all m. We will now show that, in practice, this latter condition is often hard to satisfy using only standard optical fibers.

3. PHOTONIC-CRYSTAL FIBERS AS COMPONENTS OF COMPOSITE PULSE STRETCHERS

Consider a laser system that includes a pulse compressor inducing a group delay with $\theta_2 < 0$, $\theta_3 > 0$, and $\theta_4 < 0$. This type of a group-delay profile is provided,
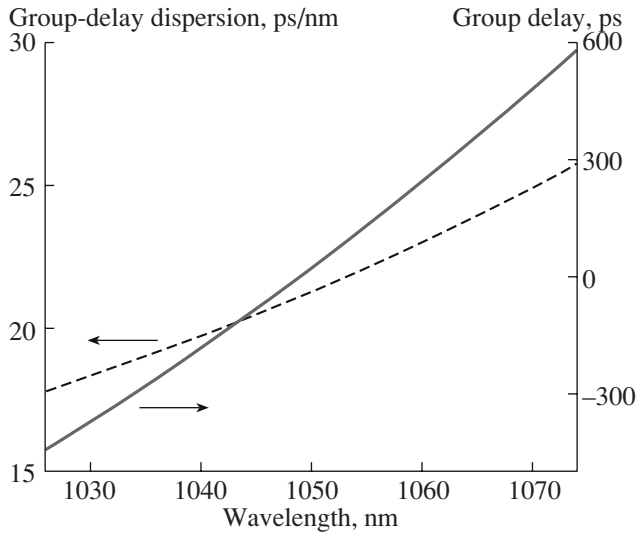
Fig. 1. Group-delay (solid line) and group-delay dispersion (dashed line) profiles of a typical grism compressor.

for example, by a standard grism compressor designed to operate with an ytterbium fiber laser output. The group-delay profile of a typical grism compressor presented in Fig. 1 corresponds to $\theta_2 \approx -12.45$ ps^2, $\theta_3 \approx 6.98 \times 10^{-2}$ ps^3, and $\theta_4 \approx -6.2 \times 10^{-4}$ ps^4 at the central wavelength $\lambda_0 = 1050$ nm. To compensate for such a group delay up to the third-order dispersion terms ($q = 3$), we reduce set (4) to two equations, $p = 2, 3$, keeping to the terms in each of the equations, $M = 2$. Solution (5) then yields $l_{1,2}^{(1)} = \Gamma_{1,2}/\Gamma$. To compensate for the group delay of the grism compressor, the overall GVD of the stretcher consisting of two fibers must be normal, which can be easily achieved at $\lambda_0 = 1050$ nm with standard optical fibers. For this type of fibers, however, the β_{3m} parameter is usually also positive (see the inset in Fig. 1). Since parameters β_{pm} are positive for $p = 2, 3$ and $m = 1, 2$), the product $l_1^{(1)} l_2^{(1)} = \Gamma_1 \Gamma_2 \Gamma^{-2}$ is always negative for the considered class of group-delay profile with $\theta_2 < 0$ and $\theta_3 > 0$. The group delay introduced by such a grism is thus difficult or impossible to precompensate with the use of standard optical fibers.

Dispersion profiles suitable for an accurate precompensation of the grism group delay can be designed by using photonic-crystal fiber technologies. These technologies, as highlighted in an earlier work, allow the dispersion profiles unattainable with standard fibers to be engineered. Here, we consider a silica–air PCF consisting of a solid core and a microstructure cladding with a large ratio of the diameter of air holes d to the pitch of the microstructure cladding Λ (see the inset in Fig. 2). To analyze the properties of the modes supported by such a waveguide structure, we employed a modification of the fully vectorial localized-function procedure [46, 47], solving the vectorial wave equa-
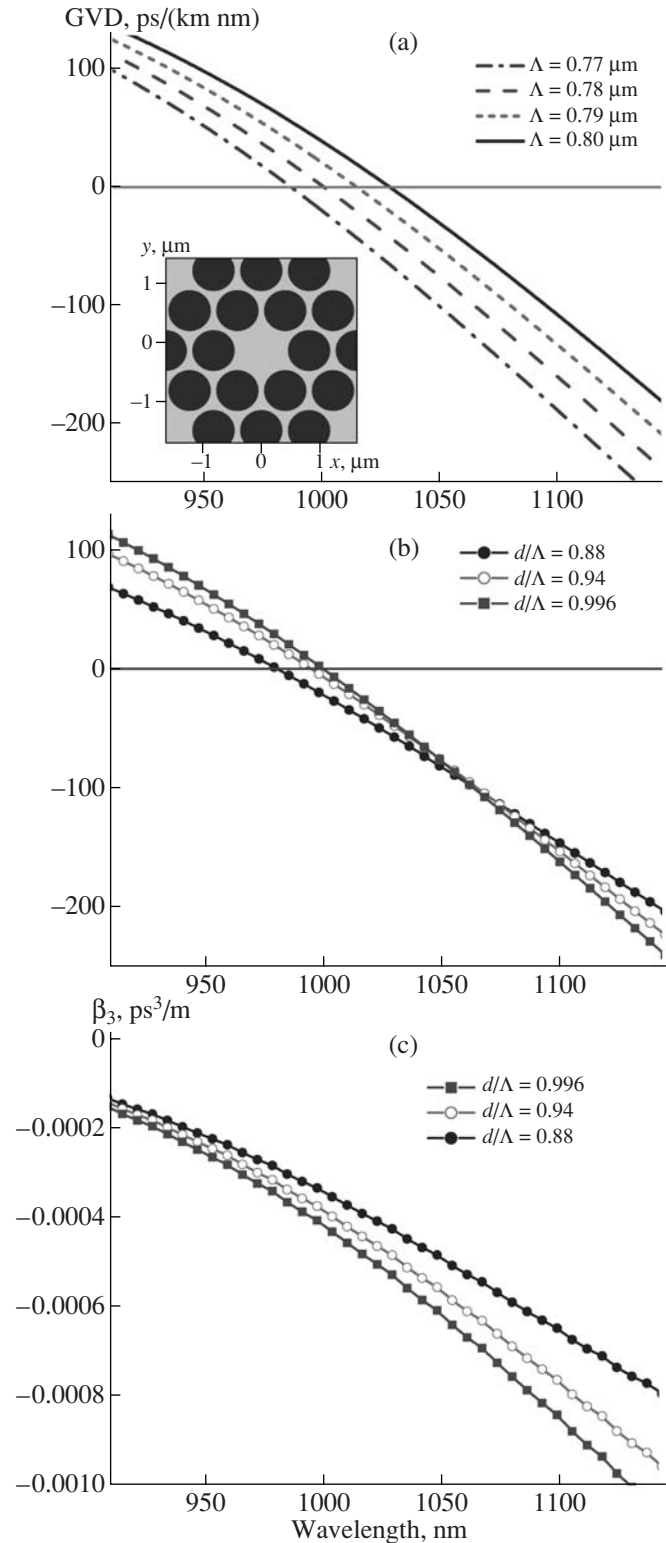

Fig. 2. Spectral profiles of the group-velocity dispersion D (a), (b) and the third-order dispersion parameter β_3 (c) as a function of the wavelength for a photonic-crystal fiber with a cross-section structure shown in the inset: (a) the pitch of the microstructure cladding Λ varies from 0.77 to 0.80 μm with $d/\Lambda = 0.996$; (b) and (c) $\Lambda = 0.78$ μm and the d/Λ ratio varies from 0.880 to 0.996.

tions for the electromagnetic field. The two-dimensional profile of the refractive index is approximated with a series expansion in the Hermite–Gaussian polynomials and trigonometric functions. Transverse components of the electromagnetic field are represented as series expansions in Hermite–Gaussian polynomials. The substitution of these series expansions for the field and refractive index into the wave equations for transverse field components reduces the problem to a matrix equation eigenfunction and eigenvalue problem, allowing the propagation constants and transverse field profiles to be determined for the PCF modes.

For sufficiently small Λ, corresponding to a small-size fiber core, the dispersion parameter $\beta_2 = \partial^2\beta/\partial\omega^2$ (and the related group-velocity dispersion parameter $D = -2\pi c\lambda^{-2}\beta_2$) of such a fiber passes through zero twice [48]. For a PCF with an extreme value of $d/\Lambda = 0.996$, the second long-wavelength zero-GVD point λ_z can be tuned from approximately 970 to 1035 nm by varying the pitch of the cladding Λ from 0.77 to 0.80 µm (Fig. 2a). For wavelengths longer than λ_z, the considered type of PCF provides the regime of normal dispersion ($\beta_2 > 0$, $D < 0$) with $\beta_3 = \partial^3\beta/\partial\omega^3 < 0$, as required for the precompensation of the grism group delay. As illustrated by the results of the calculations presented in Figs. 2b and 2c, both the β_2 and β_3 parameters can be adjusted for the optimal compensation of the target group delay by varying the d/Λ ratio.

4. NUMERICAL MODEL FOR PULSE-STRETCHING DYNAMICS

We now proceed with a numerical analysis of the spectral and temporal evolution of a laser pulse in a stretcher consisting of a sequence of optical fibers. Our numerical procedure is based on the solution of the generalized nonlinear Schrödinger equation [49, 50] for the field envelope $A = A(z, t)$:

$$
\frac{\partial A}{\partial \xi} = -\frac{\alpha^{(0)}}{2}A - i\frac{\alpha^{(1)}}{2}\frac{\partial A}{\partial \tau}
$$
$$
+ i\sum_{k=2}^{6}\frac{(i)^k}{k!}\left(\beta^{(k)} + i\frac{\alpha^{(k)}}{2}\right)\frac{\partial^k A}{\partial \tau^k} + P_{nl}(\xi, \tau),
$$
(8)

where z is the propagation coordinate, t is the time variable, τ is the retarded time, $\alpha^{(k)} = \text{Im}[\partial^k\beta/\partial\omega^k]$ accounts for the fiber loss, and $\beta^{(k)} = \text{Re}[\partial^k\beta/\partial\omega^k]$ are the coefficients in the Taylor-series expansion of the propagation constant β. The nonlinear polarization $P_{nl}(\xi, \tau)$ in Eq. (8) is defined as

$$
P_{nl}(\xi, \tau) = i\hat{F}^{-1}\left[\frac{n_2\omega}{cS_{\text{eff}}(\omega)}\tilde{P}_{nl}(\xi, \omega_0 - \omega)\right], \quad (9)
$$

where n_2 is the nonlinear refractive index of the fiber material, ω is the current frequency, ω_0 is the central frequency of the input field, c is the speed of light,

$$
S_{\text{eff}}(\omega) = \frac{\left[\int\limits_{-\infty}^{\infty}\int\limits_{-\infty}^{\infty}|F(x, y)|^2 dx dy\right]^2}{\int\limits_{-\infty}^{\infty}\int\limits_{-\infty}^{\infty}|F(x, y)|^4 dx dy} \quad (10)
$$

is the frequency-dependent effective mode area, and the operator $\hat{F}^{-1}(\bullet)$ denotes the inverse Fourier transform, $\hat{F}[f(x)] = (2\pi)^{-1/2}\int_{-\infty}^{\infty}f(x)\exp(ixy)dx$, $\hat{F}^{-1}[f(x)] = (2\pi)^{-1/2}\int_{-\infty}^{\infty}f(x)\exp(-ixy)dx$, and $\hat{F}^{-1}\{\hat{F}[f(x)]\} = f(x)$. The frequency-domain nonlinear polarization in Eq. (9) is defined through the direct Fourier transform

$$
\tilde{p}_{nl}(\xi, \omega - \omega_0) = \hat{F}\left[A(\xi, \tau)\int\limits_{-\infty}^{\infty}R(t)|A(\xi, \tau - t)|^2 dt\right], \quad (11)
$$

including both the instantaneous, Kerr nonlinearity, and the retarded Raman contribution via the nonlinear response function

$$
R(t) = (1 - f_R)\delta(t) + f_R\Theta(t)\frac{\tau_1^2 + \tau_2^2}{\tau_1\tau_2^2}e^{-\frac{t}{\tau_2}}\sin\left(\frac{t}{\tau_1}\right),
$$

where f_R is the fractional contribution of the Raman response; $\delta(t)$ and $\Theta(t)$ are the delta and the Heaviside step functions, respectively; and τ_1 and τ_2 are the characteristic times of the Raman response of the fiber material. For fused silica, $f_R = 0.18$, $\tau_1 = 12.5$ fs, and $\tau_2 = 32$ fs.

The nonlinear polarization $P_{nl}(\xi, \tau)$ defined in the form of Eq. (9) not only helps to include the influence of the frequency-dependent effective mode area S_{eff} on the nonlinear coefficient $\gamma = (n_2\omega)/(cS_{\text{eff}})$, but also yields the correct definition of the local field intensity [51], which also depends on $S_{\text{eff}}(\omega)$.

5. A TWO-STAGE FIBER-PULSE STRETCHER

We consider a two-stage stretcher consisting of a sequence of two optical fibers. For the first stage, we use a standard fiber with the parameters typical of an HI1060 fiber: $D = -45$ ps/(nm km) and $\beta_{31} = 2 \times 10^{-4}$ ps³/m at $\lambda_0 = 1050$ nm. The effective mode area for this fiber at λ_0 is $S_{1\text{eff}} \approx 30.2$ µm², corresponding to the nonlinear coefficient $\gamma_1 \approx 6.3$ W⁻¹ km⁻¹. The photonic-crystal fiber with $\Lambda = 0.78$ µm and $d/\Lambda = 0.94$ is employed as the second stage of our stretcher. The dispersion properties of this fiber (see Figs. 2b, 2c) at $\lambda_0 = 1050$ nm are characterized by the parameters $\beta_{22} = 4.56 \times 10^{-2}$ ps²/m, $\beta_{32} = -5.58 \times 10^{-4}$ ps³/m, and $\beta_{42} = 1.98 \times 10^{-6}$ ps⁴/m. The fourth-order dispersion of the first fiber is assumed

to be negligible with respect to the fourth-order dispersion of the PCF $\beta_{41} \ll \beta_{42}$. This assumption reflects the realistic relation between the dispersion parameters of the standard and photonic-crystal fibers considered in this work. The effective mode area for the fundamental mode of PCF at λ_0 is $S_{2\text{eff}} \approx 0.57\ \mu m^2$, corresponding to a very high nonlinearity of $\gamma_2 \approx 330\ W^{-1}\ km^{-1}$. We also include a loss of 100 dB/km to account for inevitable limitations of fiber technologies when applied to the fabrication of fibers with such a small core.

Since the second fiber possesses a very high nonlinearity, as a penalty for the unusual dispersion profile, which is required for the accurate dispersion compensation, the key function of the first fiber is to stretch the pulse before it enters the highly nonlinear PCF in order to reduce the nonlinear phase shift in the second fiber. We will include the nonlinear effects iteratively showing that the nonlinear phase shift can partially balance the fourth-order dispersion of the fiber stretcher.

To demonstrate the convergence of the proposed stretcher design algorithm to a target dispersion profile, we examine the propagation dynamics for laser pulses with two representative sets of input parameters. Input pulses of the first type will have the pulse width $\tau_{p1} = 200$ fs and the input pulse energy $W_1 = 400$ pJ. For input pulses of the second type, we set $\tau_{p2} = 100$ fs and $W_2 = 50$ pJ. Such a comparative analysis will show that, for shorter input pulses, the stretcher design becomes progressively more difficult requiring a larger number of iterations. In accordance with Eq. (5), the fiber lengths are chosen equal to $l_1^{(1)} \approx 169.6$ m and $l_2^{(1)} \approx 159.1$ m in the first iteration of our procedure. To compensate for the loss in the PCF, we include an amplification with a gain of 0.5 dB/m within the first 15 m of the first fiber for the input pulses of the first type and a gain of 1.47 dB/m within the first 10 m of the first fiber for the input pulses of the second type.

Figures 3a and 3b display the spectra of laser pulses of the first and second type after the amplification in the initial section of the first fiber (solid line), at the output of the first fiber (dashed line) and at the output of the PCF (dash–dotted line). The energy of the laser pulses after the amplification segment is 2.24 and 1.48 nJ for the first and second types of input pulses, respectively. At the output of the stretcher, the energies of the first and second types of laser pulses are approximately 50.0 and 31.5 pJ, respectively. As can be seen from the time-domain dynamics of pulse stretching (Figs. 4a, 4b), the first fiber stretches the input pulse up to hundreds of picoseconds (field snapshots at 169.6 m), reducing the nonlinear effects in the highly nonlinear PCF employed for the second stage of the pulse stretcher. As a result, the propagation through the PCF is accompanied by virtually no changes in the spectrum of the light pulse (Figs. 3a, 3b).
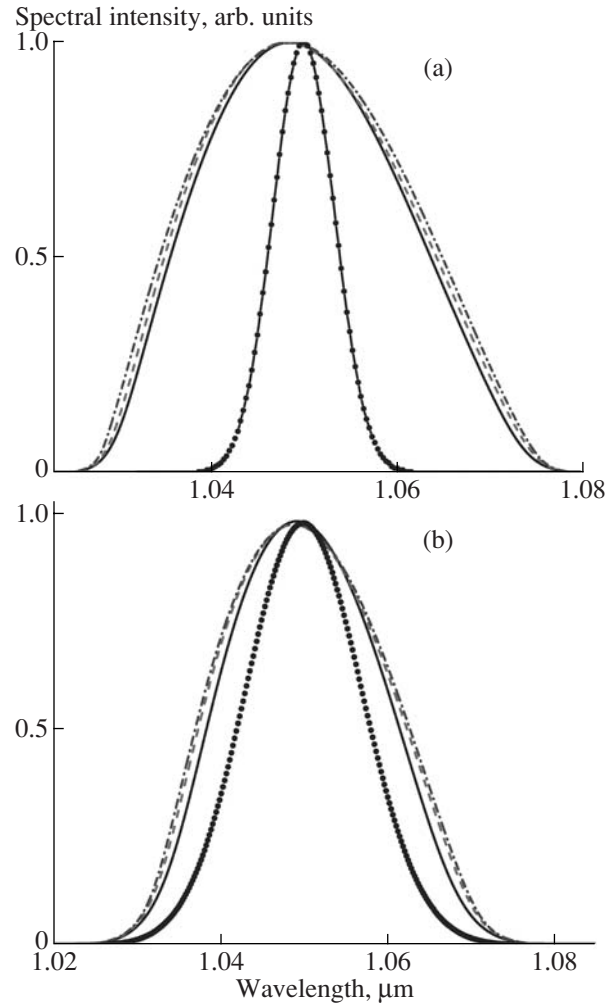

Fig. 3. The spectral evolution of laser pulses in the fiber stretcher after amplification in the initial section of the first fiber (solid line), at the output of the first fiber (dashed line), and at the output of the PCF (dash–dotted line). The input pulse width is (a) 200 and (b) 100 fs. The input energy is (a) 400 and (b) 50 pJ. All of the spectra are normalized to their peak values. The filled circles show the spectrum of the input pulse.

6. NONLINEAR PHASE SHIFT IN A COMPOSITE FIBER PULSE STRETCHER

Within the initial section of the pulse stretcher, where the pulse width is still short and the pulse peak power is high, the laser field acquires a nonlinear phase shift. Although this phase shift is sensitive to the parameters of the input laser pulse, the analysis presented below in this section helps to identify significant general tendencies in the modification of the spectral phase due to nonlinear effects and to propose a generic strategy for a partial compensation of the resulting pulse distortions. The nonlinear spectral phase $\Phi^{(1)}$ originating from the nonlinear spectral shift and the related nonlinear group delay $\Theta^{(1)} = \partial\Phi^{(1)}/\partial\omega$ for the first and second types of input laser pulses considered here are
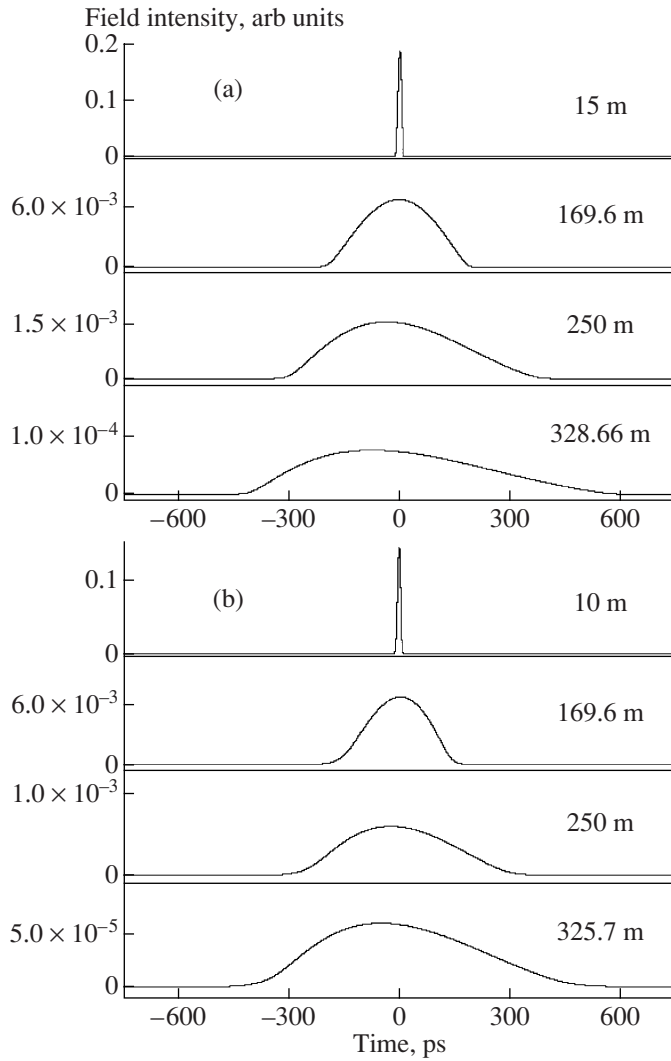
Field intensity, arb units

Fig. 4. Time-domain evolution of laser pulses in the fiber stretcher after amplification in the initial section of the first fiber (15 m), at the output of the first fiber (169.6 m), at a distance of 250 m from the input of the stretcher, and at the output of the stretcher (328.66 m). The input pulse width is (a) 200 and (b) 100 fs. The input energy is (a) 400 and (b) 50 pJ.

shown in Figs. 5a and 5b. The group-delay dispersion $\psi_2^{(j)} = \partial^2 \Phi^{(j)}/\partial\omega^2$ induced by the optical nonlinearity at the first step of our iterative procedure can be approximated by a Taylor-series expansion about the central wavelength of 1050 nm:

$$\psi_2^{(1)}(\omega) \approx \xi_2^{(1)} + \xi_3^{(1)}(\omega - \omega_0) + \frac{\xi_4^{(1)}}{2}(\omega - \omega_0)^2 + \dots, \quad (12)$$

where $\xi_k^{(1)} = (\partial^k \Phi^{(1)}/\partial\omega^k)_{\omega_0}$.

For the first and second types of input laser pulses, the spectral profiles of $\psi_2^{(1)}$ and $\psi_3^{(1)} = \partial^3\Phi^{(1)}/\partial\omega^3$ are presented in Figs. 6a and 6b. At $\lambda_0 = 1050$ nm, we find
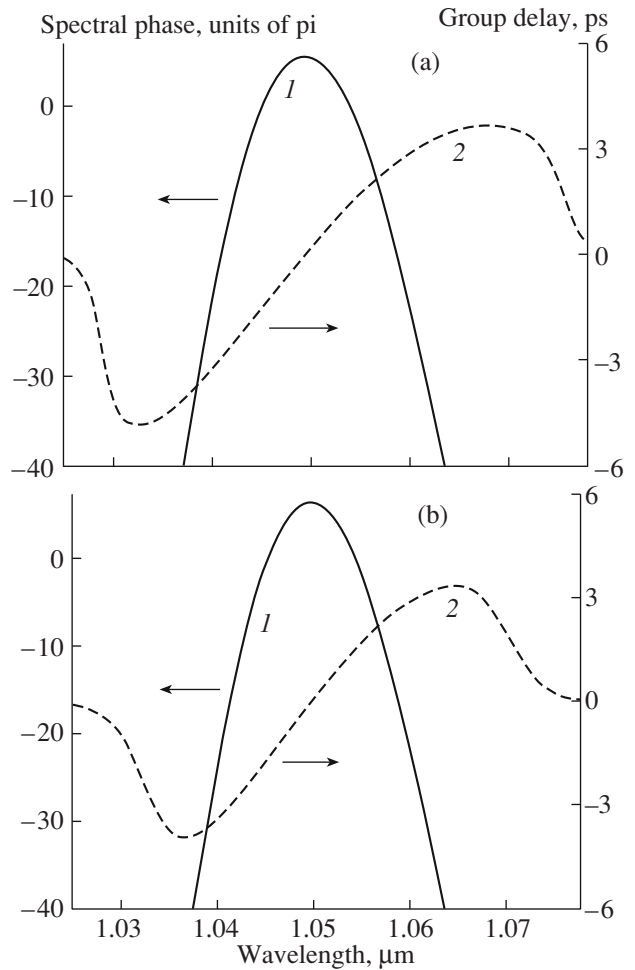

Fig. 5. Spectral profiles of the nonlinear spectral phase $\Phi^{(1)}$ (curve *1*) and the group delay $\Theta^{(1)}$ induced by a nonlinearity (curve *2*) for a laser pulse transmitted through the fiber stretcher. The input pulse width is (a) 200 and (b) 100 fs. The input energy is (a) 400 and (b) 50 pJ.

$\xi_2^{(1)} \approx -0.191$ ps², $\xi_3^{(1)} \approx -2.92 \times 10^{-3}$ ps³, and $\xi_4^{(1)} \approx 2.93 \times 10^{-4}$ ps⁴ for the input pulses of the first type and $\xi_2^{(1)} \approx -0.206$ ps², $\xi_3^{(1)} \approx -2.86 \times 10^{-3}$ ps³, and $\xi_4^{(1)} \approx 3.90 \times 10^{-4}$ ps⁴ for the input pulses of the second type.

In the first iteration of our procedure, described by Eqs. (4)–(7), nonlinear effects give rise to uncompensated phase shifts, which translate into the residual group delay $\Delta^{(1)}(\omega) = G_s^{(1)}(\omega) + \Theta^{(1)}(\omega) - G_c(\omega)$ of the stretcher–compressor system, distorting light pulses at the output of the pulse compressor. This uncompensated group delay can be represented as a Taylor-series expansion about ω_0:

$$\Delta^{(1)}(\omega) \approx \delta\beta_2^{(1)}(\omega - \omega_0) + \frac{\delta\beta_3^{(1)}}{2}(\omega - \omega_0)^2$$
$$+ \frac{\delta\beta_4^{(1)}}{6}(\omega - \omega_0)^3 + \dots. \quad (13)$$

Here, at $\lambda_0 = 1050$ nm, $\delta\beta_2^{(1)} \approx \xi_2^{(1)}$, $\delta\beta_3^{(1)} \approx \xi_3^{(1)}$, and $\delta\beta_4^{(1)} \approx \theta_4 + \beta_{42}l_2^{(1)} + \xi_4^{(1)}$.

The key result of the first-iteration analysis is that the nonlinear phase shift can partially compensate for the fourth-order fiber dispersion. In the case considered here, we find $\delta\beta_4^{(1)} \approx 3.0 \times 10^{-6}$ ps^4, which is two orders of magnitude less than $\xi_4^{(1)} \approx 3.90 \times 10^{-4}$ ps^4. This important finding allows the desired dispersion profile of a fiber stretcher to be designed with an accuracy up to the fourth-order dispersion terms using a sequence of only two optical fibers, as in the example considered throughout this paper.

7. AN ITERATIVE DESIGN OF A FIBER STRETCHER DISPERSION PROFILE

To minimize the residual group delay originating from nonlinear phase shifts, we include the nonlinear effects into the stretcher design rule at the second step of our iterative procedure. To this end, we represent the group-delay dispersion $\psi_2^{(j)} = \partial^2\Phi^{(j)}/\partial\omega^2$ induced by the optical nonlinearity at the jth step of our iterative procedure as a Taylor-series expansion about the central wavelength of 1050 nm:

$$\psi_2^{(j)}(\omega) \approx \xi_2^{(j)} + \xi_3^{(j)}(\omega - \omega_0) + \frac{\xi_4^{(j)}}{2}(\omega - \omega_0)^2 + \dots, \quad (14)$$

where $\xi_k^{(j)} = (\partial^k\Phi^{(j)}/\partial\omega^k)_{\omega_0}$ and j stands for the number of iteration steps.

At the second step of our iteration procedure, the fiber lengths $l_m^{(2)}$ are found from the set of equations

$$\sum_{m=1}^{M}\beta_{pm}l_m^{(2)} = -(\theta_p + \xi_p^{(1)}). \quad (15)$$

The solution of Eq. (15) with $p = 2$, 3 and $m = 1$, 2 yields $l_1^{(2)} \approx 165.6$ m and $l_2^{(2)} \approx 167.3$ m for the input pulses of the first type and $l_1^{(2)} \approx 165.8$ m and $l_2^{(2)} \approx 167.5$ m for the input pulses of the second type. In this iteration ($j = 2$), parameters $\xi_k^{(j)}$ in the Taylor-series expansion of the nonlinearity-induced group-delay dispersion [Eq. (14)] about $\lambda_0 = 1050$ nm are defined as $\xi_2^{(2)} \approx -0.186$ ps^2, $\xi_3^{(2)} \approx -2.75 \times 10^{-3}$ ps^3, and $\xi_4^{(2)} \approx 2.88 \times 10^{-4}$ ps^4 for the input pulses of the first type and $\xi_2^{(2)} \approx -0.20$ ps^2, $\xi_3^{(2)} \approx -2.68 \times 10^{-3}$ ps^3, and $\xi_4^{(2)} \approx 3.83 \times 10^{-4}$ ps^4 for the input pulses of the second type.
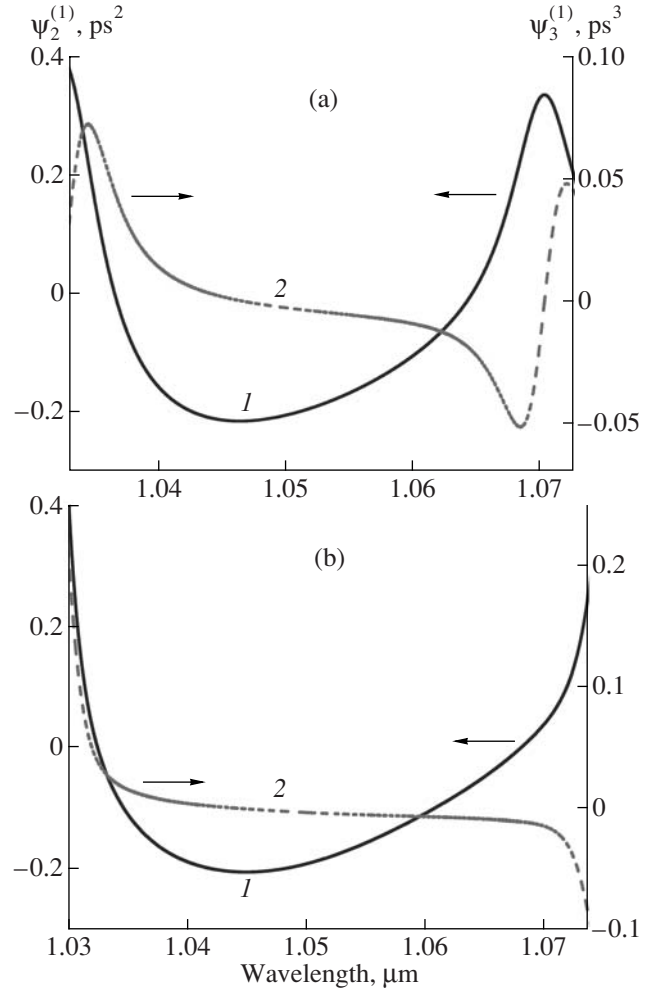
Fig. 6. Spectral profiles of parameters $\psi_2^{(1)}$ (curve *1*) and $\psi_3^{(1)}$ (curve *2*) for a laser pulse transmitted through the fiber stretcher. The input pulse width is (a) 200 and (b) 100 fs. The input energy is (a) 400 and (b) 50 pJ.

An uncompensated stretcher–compressor group delay at the jth step of our iteration procedure is represented as

$$\Delta^{(j)}(\omega) \approx \delta\beta_2^{(j)}(\omega - \omega_0) + \frac{\delta\beta_3^{(j)}}{2}(\omega - \omega_0)^2$$
$$+ \frac{\delta\beta_4^{(j)}}{6}(\omega - \omega_0)^3 + \dots. \quad (16)$$

Here, the coefficients $\delta\beta_k^{(2)}$ are given by

$$\delta\beta_2^{(j)} \approx \theta_2 + \beta_{21}l_1^{(j)} + \beta_{22}l_2^{(j)} + \xi_2^{(j)}, \quad (17)$$

$$\delta\beta_3^{(j)} \approx \theta_3 + \beta_{31}l_1^{(j)} + \beta_{32}l_2^{(j)} + \xi_3^{(j)}, \quad (18)$$

$$\delta\beta_4^{(j)} \approx \theta_4 + \beta_{42}l_2^{(j)} + \xi_4^{(j)}. \quad (19)$$

At the second stage of our iteration procedure ($j = 2$), we find $\delta\beta_2^{(2)} \approx 5.3 \times 10^{-3}$ ps^2, $\delta\beta_3^{(2)} \approx 1.7 \times 10^{-4}$ ps^3, and $\delta\beta_4^{(2)} \approx -1.3 \times 10^{-6}$ ps^4 for the input pulses of the first type and $\delta\beta_2^{(2)} \approx 6.0 \times 10^{-3}$ ps^2, $\delta\beta_3^{(2)} \approx 1.8 \times 10^{-4}$ ps^3, and $\delta\beta_4^{(2)} \approx 1.1 \times 10^{-4}$ ps^4 for the second-type input pulses.

The second iteration thus improves the compensation of the second- and third-order dispersion in the stretcher–compressor system by more than an order of magnitude. Indeed, introducing the ratio $\rho_k = \left| \delta\beta_k^{(2)} / \delta\beta_k^{(1)} \right|$ to quantify the improvement in the second- and third-order dispersion compensation ($k = 2, 3$) by the second iteration in our procedure, we find $\rho_2 \approx 0.028$ and $\rho_3 \approx 0.058$ for the input pulses of the first type and $\rho_2 \approx 0.03$ and $\rho_3 \approx 0.063$ for the input pulses of the second type.

We now continue our iterative procedure by including the coefficients $\xi_k^{(j)}$ from the jth iteration into the equations for the fiber lengths $l_m^{(j+1)}$ to adjust the fiber lengths for the best compensation of the second- and third-order dispersion:

$$\sum_{m=1}^{M} \beta_{pm} l_m^{(j+1)} = -(\theta_p + \xi_p^{(j)}), \qquad (20)$$

where $p = 2, 3, \ldots, q + 1$, with q being the maximum order of dispersion to be compensated. The solution to Eq. (20) is given by

$$l_i^{(j+1)} = \frac{D_i^{(j+1)}}{D}, \qquad (21)$$

where

$$D_i^{(j+1)} = \begin{vmatrix} \beta_{21} & \cdots & \beta_{2i-1} & -\theta_2 - \xi_2^{(j)} & \beta_{2i+1} & \cdots & \beta_{2M} \\ \beta_{31} & \cdots & \beta_{3i-1} & -\theta_3 - \xi_3^{(j)} & \beta_{3i+1} & \cdots & \beta_{3M} \\ \cdots & \cdots & \cdots & \cdots & \cdots & \cdots & \cdots \\ \beta_{q1} & \cdots & \beta_{qi-1} & -\theta_q - \xi_q^{(j)} & \beta_{qi+1} & \cdots & \beta_{qM} \end{vmatrix} \quad (22)$$

is the determinant of the matrix obtained from $\hat{\beta}_{pm}$ by replacing the ith column by the column composed of the free terms $-\theta_p - \xi_p^{(j)}$ in set of Eqs. (20).

To compensate for the stretcher–compressor dispersion up to the third order ($q = 3$), we set $p = 2, 3$ and $M = 2$ as before. Solution (21) then reduces to

$$l_1^{(j+1)} = \frac{\beta_{32}[\theta_2 + \xi_2^{(j)}] - \beta_{22}[\theta_3 + \xi_3^{(j)}]}{\beta_{31}\beta_{22} - \beta_{21}\beta_{32}}, \qquad (23)$$

$$l_2^{(j+1)} = \frac{\beta_{31}[\theta_2 + \xi_2^{(j)}] - \beta_{21}[\theta_3 + \xi_3^{(j)}]}{\beta_{31}\beta_{22} - \beta_{21}\beta_{32}}. \qquad (24)$$

After the third iteration ($j = 3$), we have $\delta\beta_2^{(3)} \approx 1.0 \times 10^{-5}$ ps^2, $\delta\beta_3^{(3)} \approx -8.0 \times 10^{-6}$ ps^3, and $\delta\beta_4^{(3)} \approx 2.0 \times 10^{-7}$ ps^4 for the input pulses of the first type and $\delta\beta_2^{(3)} \approx 1.5 \times 10^{-4}$ ps^2, $\delta\beta_3^{(3)} \approx -1.0 \times 10^{-5}$ ps^3, and $\delta\beta_4^{(3)} \approx 1.1 \times 10^{-4}$ ps^4 for the second-type input pulses. This gives a nearly perfect stretcher–compressor group-delay compensation for the input pulses of the first type (Fig. 7a). For the second-type input pulses, a noticeable improvement in the stretcher–compressor dispersion compensation can be achieved by the fourth iteration (Fig. 7b), yielding $\delta\beta_2^{(4)} \approx 4.0 \times 10^{-5}$ ps^2, $\delta\beta_3^{(4)} \approx -5.0 \times 10^{-6}$ ps^3, and $\delta\beta_4^{(4)} \approx 1.1 \times 10^{-4}$ ps^4.

8. SHORT LASER PULSES IN OPTIMIZED STRETCHER–COMPRESSOR SYSTEMS

Due to the optical nonlinearity of the pulse stretcher, the spectrum of a laser pulse at the output of the stretcher–compressor system is noticeably broader than the spectrum of the input pulse (Figs. 4a, 4b). The joint action of the third-order dispersion and fiber nonlinearity gives rise to a slight asymmetry of the output spectrum. In the time domain, the unbalanced dispersion of the stretcher–compressor system and nonlinear effects generally distort the output pulse. However, the proposed strategy of the fiber stretcher design allows these distortions to be minimized through a careful optimization of the structure of the PCF used at the second stage of the stretcher and the proper choice of the fiber lengths.

As shown in Fig. 8, each iteration of the above-described procedure reduces the pulse distortions at the output of a stretcher–compressor system. For input pulses of the first type (Fig. 8a), a fiber stretcher optimized through a three-step iteration process permits the generation of a nearly Gaussian pulse at the output of the grism compressor. Due to the nonlinearity-induced spectral broadening of the laser pulse in the stretcher, the temporal width of the output pulse in this case (about 80 fs) is substantially shorter than the input pulse width (200 fs). Because of the losses in the PCF, the peak power of the output pulse in Fig. 8a is approximately three times lower than the peak power of the input pulse. For input pulses of the second type (Fig. 8b), the stretcher optimization enables the formation of a compressor output with a low-energy pedestal with most of the field energy concentrated within the central peak, whose duration is approximately equal to the pulse width of the input pulse. The peak power of the output pulse is approximately two times lower than the peak power of the input pulse.
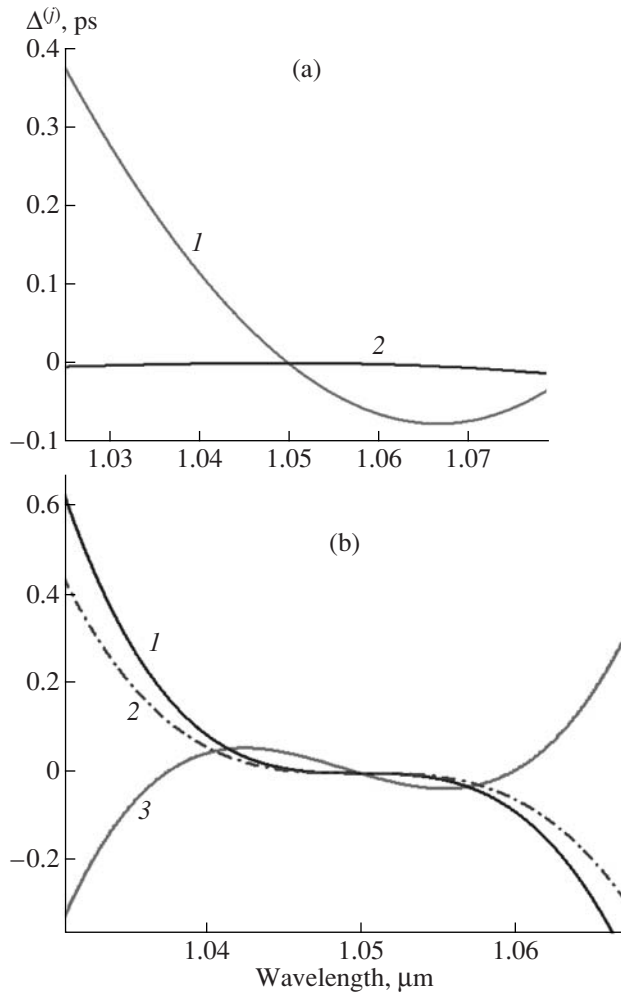
Fig. 7. Spectral profile of the uncompensated stretcher–compressor group delay $\Delta^{(j)}$: (a) the input pulse width is 200 fs, the input energy is 400 pJ, $j = 2$ (*1*), and 3 (*2*); (b) the input pulse width is 100 fs, the input energy is 50 pJ, $j = 2$ (*1*), 3 (*2*), and 4 (*3*).

Fig. 8. Intensity envelope at the output of the stretcher–compressor system: (a) the input pulse width is 200 fs, the input energy is 400 pJ, $j = 2$ (*1*), and 3 (*2*), the input pulse envelope is shown by curve *3*; (b) the input pulse width is 100 fs, the input energy is 50 pJ, $j = 2$ (*1*), 3 (*2*), and 4 (*3*), the input pulse envelope is shown by curve *4*.

While we mainly focused in this work on the processes that are of critical importance for the design of a PCF-based stretcher for a fiber laser system, we expect that the design rules for the overall oscillator–stretcher–amplifier–compressor system should be sensitive to such additional factors as optical nonlinearities and gain spectral effects in the fiber amplifier chain, as well as the PCF fabrication tolerances. In particular, with light pulses amplified to maximum attainable levels, the additional self-phase modulation on top of the chirped pulses may give rise to additional effective dispersion orders, which may require additional iterations in the stretcher optimization procedure. The role of the gain spectral effects in the fiber amplifier chain is twofold. On the one hand, gain narrowing in the amplifier stage may impose an additional limitation on the output pulse width. On the other hand, due to this spectral nar-
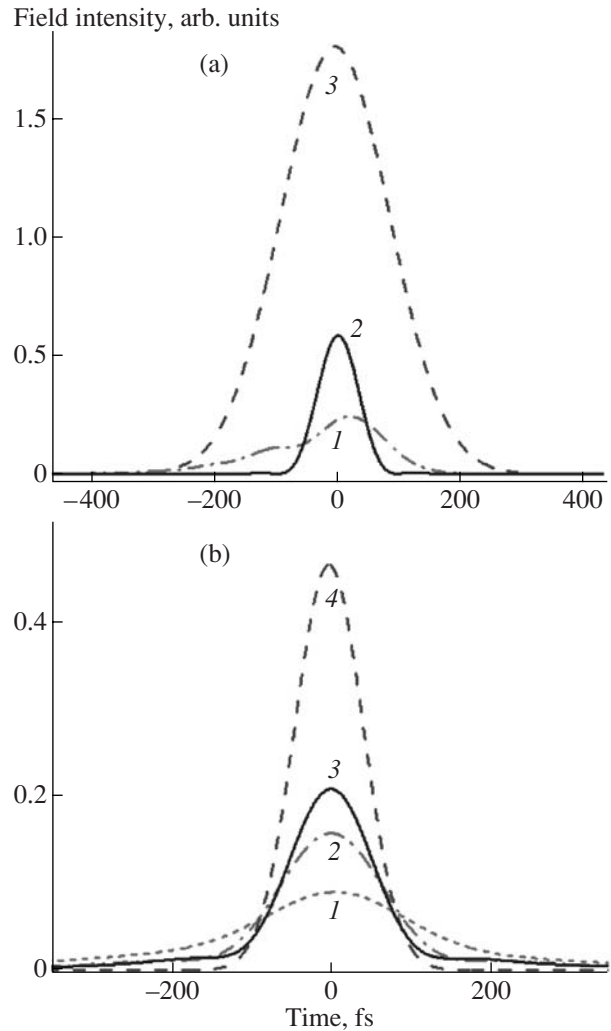
rowing before the final compression stage, some of the nonlinear phase compensation considered above might not be needed. Finally, the methods of compensating for inaccuracies in the PCF fabrication include variations in the fiber lengths, input pulse parameters, and adjustment of the grism compressor.

9. CONCLUSIONS

The analysis presented in this work shows that PCFs with a specifically designed dispersion profile and nonlinearity allow an accurate broadband compensation of the group delay originating from the functional components in fiber oscillator–amplifier sources of high-peak-power ultrashort light pulses involving pulse stretching, chirped-pulse amplification, and pulse compression. We show that, for a broad class of such systems, the

nonlinear phase shift can partially compensate for the fourth-order dispersion in a carefully optimized sequence of fibers. The developed algorithm for the design of PCF-based stretcher–compressor systems allows the group delay of a pulse compressor to be compensated to the fourth order by using a sequence of only two fibers—a standard passive fiber and a PCF. Examples of short-pulse dynamics in stretcher–compressor systems presented in this work demonstrate the performance of optimized PCF-based stretchers for the generation of high-peak-power femtosecond light pulses.

REFERENCES

1. J. C. Knight, T. A. Birks, P. St. J. Russell, and D. M. Atkin, "All-Silica Single-Mode Optical Fiber with Photonic Crystal Cladding," Opt. Lett. **21**, 1547–1549 (1996).

2. J. C. Knight, J. Broeng, T. A. Birks, and P. St. J. Russell, "Photonic Bandgap Quidance in Optical Fibers," Science **282**, 1476–1478 (1998).

3. P. St. J. Russell, "Photonic Crystal Fibers," Science **299**, 358–362 (2003).

4. J. C. Knight, "Photonic Crystal Fibers," Nature **424**, 847–851 (2003).

5. W. H. Reeves, D. V. Skryabin, F. Biancalana, et al., "Transformation and Control of Ultra-Short Pulses in Dispersion-Engineered Photonic Crystal Fibres," Nature **424**, 511–515 (2003).

6. W. J. Wadsworth, A. Ortigosa-Blanch, J. C. Knight, et al., "Supercontinuum Generation in Photonic Crystal Fibers and Optical Fiber Tapers: a Novel Light Source," J. Opt. Soc. Am. B **19**, 2148–2155 (2002).

7. A. M. Zheltikov, "Nonlinear Optics of Microstructure Fibers," Phys. Usp. **47**, 69–98 (2004).

8. A. B. Fedotov, A. M. Zheltikov, A. P. Tarasevitch, and D. von der Linde, "Enhanced Spectral Broadening of Short Laser Pulses in High-Numerical-Aperture Holey Fibers," Appl. Phys. B **73**, 181–184 (2001).

9. J. C. Travers, R. E. Kennedy, S. V. Popov, et al., "Extended Continuous-Wave Supercontinuum Generation in a Low-Water-Loss Holey Fiber," Opt. Lett. **30**, 1938–1940 (2005).

10. E. E. Serebryannikov, A. M. Zheltikov, N. Ishii, et al., "Nonlinear-Optical Spectral Transformation of Few-Cycle Laser Pulses in Photonic-Crystal Fibers," Phys. Rev. E **72**, 056603 (2005).

11. J. K. Ranka, R. S. Windeler, and A. J. Stentz, "Visible Continuum Generation in Air-Silica Microstructure Optical Fibers with Anomalous Dispersion at 800 nm," Opt. Lett. **25**, 25–27 (2000).

12. A. M. Zheltikov, "Let there be White Light: Supercontinuum Generation by Ultrashort Laser Pulses," Phys. Usp. **49**, 605–628 (2006).

13. D. J. Jones, S. A. Diddams, J. K. Ranka, et al., "Carrier-Envelope Phase Control of Femtosecond Mode-Locked Lasers and Direct Optical Frequency Synthesis," Science **288**, 635–639 (2000).

14. R. Holzwarth, T. Udem, T. W. Hänsch, et al., "Optical Frequency Synthesizer for Precision Spectroscopy," Phys. Rev. Lett. **85**, 2264–2267 (2000).

15. S. A. Diddams, D. J. Jones, Jun Ye, et al., "Direct Link between Microwave and Optical Frequencies with a 300 THz Femtosecond Laser Comb," Phys. Rev. Lett. **84**, 5102 (2000).

16. Th. Udem, R. Holzwarth, and T.W. Hänsch, "Optical Frequency Metrology," Nature **416**, 233–237 (2002).

17. I. Hartl, X. D. Li, C. Chudoba, et al., "Ultrahigh-Resolution Optical Coherence Tomography Using Continuum Generation in an Air-Silica Microstructure Optical Fiber," Opt. Lett. **26**, 608–610 (2001).

18. S. O. Konorov, D. A. Akimov, E. E. Serebryannikov, et al., "Cross-Correlation FROG CARS with Frequency-Converting Photonic-Crystal Fibers," Phys. Rev. E **70**, 057601 (2004).

19. D. A. Sidorov-Biryukov, E. E. Serebryannikov, and A. M. Zheltikov, "Time-Resolved Coherent Anti-Stokes Raman Scattering with a Femtosecond Soliton Output of a Photonic-Crystal Fiber," Opt. Lett. **31**, 2323–2325 (2006).

20. H. N. Paulsen, K. M. Hilligsøe, J. Thøgersen, et al., "Coherent Anti-Stokes Raman Scattering Microscopy with a Photonic Crystal Fiber Based Light Source," Opt. Lett. **28**, 1123–1125 (2003).

21. H. Kano and H. Hamaguchi, "Vibrationally Resonant Imaging of a Single Living Cell by Supercontinuum-Based Multiplex Coherent Anti-Stokes Raman Scattering Microspectroscopy," Opt. Express **13**, 1322–1327 (2005).

22. B. von Vacano, W. Wohlleben, and M. Motzkus, "Actively Shaped Supercontinuum from a Photonic Crystal Fiber for Nonlinear Coherent Microspectroscopy," Opt. Lett. **31**, 413–415 (2006).

23. S. Konorov, A. Ivanov, D. Ivanov, et al., "Ultrafast Photonic-Crystal Fiber Light Flash for Streak-Camera Fluorescence Measurements," Opt. Express **13**, 5682–5688 (2005).

24. A. Baltuška, T. Fuji, and T. Kobayashi, "Self-Referencing of the Carrier-Envelope Slip in a 6-fs Visible Parametric Amplifier," Opt. Lett. **27**, 1241–1243 (2002).

25. R. Kienberger, E. Goulielmakis, M. Uiberacker, et al., "Atomic Transient Recorder," Nature **427**, 817–821 (2004).

26. A. Baltuška, Th. Udem, M. Uiberacker, et al., "Attosecond control of electronic processes by intense light fields," Nature **421**, 611–615 (2003).

27. A. Baltuška, M. Uiberacker, E. Goulielmakis, et al., "Phase Controlled Amplification of Few-Cycle Laser

Pulses," IEEE J. Sel. Top. Quantum Electron. **9**, 972–989 (2003).

28. Ch. Gohle, Th. Udem, J. Rauschenberger, et al., "A Frequency Comb in the Extreme Ultraviolet," Nature **436**, 234–237 (2005)

29. H. Lim, F. Ilday, and F. Wise, "Femtosecond Ytterbium Fiber Laser with Photonic Crystal Fiber for Dispersion Control," Opt. Express **10**, 1497–1502 (2002).

30. H. Lim and F. Wise, "Control of Dispersion in a Femtosecond Ytterbium Laser by Use of Hollow-Core Photonic Bandgap Fiber," Opt. Express **12**, 2231–2235 (2004).

31. H. Lim, A. Chong, and F. W. Wise, "Environmentally-Stable Femtosecond Ytterbium Fiber Laser with Birefringent Photonic Bandgap Fiber," Opt. Express **13**, 3460–3464 (2005).

32. A. Isomäki and O. G. Okhotnikov, "All-Fiber Ytterbium Soliton Mode-Locked Laser with Dispersion Control by Solid-Core Photonic Bandgap Fiber," Opt. Express **14**, 4368–4373 (2006).

33. C. K. Nielsen, K. G. Jespersen, and S. R. Keiding, "A 158 fs 5.3 nJ Fiber-Laser System at 1 μm Using Photonic Bandgap Fibers for Dispersion Control and Pulse Compression," Opt. Express **14**, 6063–6068 (2006).

34. T. Schreiber, C. K. Nielsen, B. Ortac, et al., "Microjoule-Level All-Polarization-Maintaining Femtosecond Fiber Source," Opt. Lett. **31**, 574–576 (2006).

35. J. Limpert, A. Liem, M. Reich, et al., "Low-Nonlinearity Single-Transverse-Mode Ytterbium-Doped Photonic Crystal Fiber Amplifier," Opt. Express **12**, 1313–1319 (2004).

36. T. Südmeyer, F. Brunner, E. Innerhofer, et al., "Nonlinear Femtosecond Pulse Compression at High Average Power Levels by Use of a Large-Mode-Area Holey Fiber," Opt. Lett. **28**, 1951–1953 (2003).

37. J. Limpert, T. Schreiber, S. Nolte, et al., "All Fiber Chirped-Pulse Amplification System Based on Compression in Air-Guiding Photonic Bandgap Fiber," Opt. Express **11**, 3332–3337 (2003).

38. C. J. S. de Matos, S. V. Popov, A. B. Rulkov, et al., "All-Fiber Format Compression of Frequency Chirped Pulses in Air-Guiding Photonic Crystal Fibers," Phys. Rev. Lett. **93**, 103901 (2004).

39. C. D. Brooks and F. Di Teodoro, "Multimegawatt Peak-Power, Single-Transverse-Mode Operation of a 100 μm Core Diameter, Yb-Doped Rodlike Photonic Crystal Fiber Amplifier," Appl. Phys. Lett. **89**, 111119 (2006).

40. A. Galvanauskas, "Mode-Scalable Fiber-Based Chirped Pulse Amplification Systems," IEEE J. Sel. Top. Quantum Electron. **7**, 504 (2001).

41. A. Galvanauskas, "High Power Fiber Lasers," Opt. Photon. News **15**, 42–47 (2004).

42. J. C. Knight, T. A. Birks, R. F. Cregan, et al., "Large Mode Area Photonic Crystal Fibre," Electron. Lett. **34**, 1347 (1998).

43. K. Furusawa, A. Malinowski, J. Price, et al., "Cladding Pumped Ytterbium-Doped Fiber Laser with Holey Inner and Outer Cladding," Opt. Express **9**, 714–720 (2001).

44. W. Wadsworth, R. Percival, G. Bouwmans, et al., "High Power Air-Clad Photonic Crystal Fibre Laser," Opt. Express **11**, 48–53 (2003).

45. J. Limpert, T. Schreiber, S. Nolte, et al., "High-Power Air-Clad Large-Mode-Area Photonic Crystal Fiber Laser," Opt. Express **11**, 818–823 (2003).

46. G. Genty, T. Ritari, and H. Ludvigsen, "Supercontinuum Generation in Large Mode-Area Microstructured Fibers," Opt. Express **13**, 8625–8633 (2005).

47. A. V. Mitrofanov, A. A. Ivanov, A. A. Podshivalov, et al., JETP Lett. (in press).

48. T. M. Monro, D. J. Richardson, N. G. R. Broderick, and P. J. Bennet, "Modelling Large Air Fraction Holey Optical Fibers," J. Lightwave Technol. **18**, 50–56 (2000).

49. E. E. Serebryannikov, D. von der Linde, and A. M. Zheltikov, "Phase-Matching Solutions for High-Order Harmonic Generation in Hollow-Core Photonic-Crystal Fibers," Phys. Rev E **70**, 061412 (2004).

50. D. V. Skryabin, F. Luan, J. C. Knight, and P. St. J. Russell, "Soliton Self-Frequency Shift Cancellation in Photonic Crystal Fibers," Science **301**, 1705–1708 (2003).

51. K. J. Blow and D. Wood, "Theoretical Description of Transient Stimulated Raman Scattering in Optical Fibers," IEEE J. Quantum Electron. **25**, 2665–2673 (1989).

52. G. P. Agrawal, *Nonlinear Fiber Optics* (Academic, San Diego, 2001; Mir, Moscow, 1996).

53. E. E. Serebryannikov and A. M. Zheltikov, "Soliton Self-Frequency Shift with Diffraction-Suppressed Wavelength Variance and Timing Jitter," J. Opt. Soc. Am. B **23**, 1882–1887 (2006).